

Thermodynamics and Phase Diagrams of layered superconductor/ferromagnet nanostructures

Paul H. Barsic,^{1,*} Oriol T. Valls,^{1,†} and Klaus Halterman^{2,‡}

¹ *School of Physics and Astronomy, University of Minnesota, Minneapolis, Minnesota 55455[§]*

² *Physics and Computational Sciences, Research and Engineering Sciences Department, Naval Air Warfare Center, China Lake, California 93555, USA*

(Dated: April 13, 2018)

We study the thermodynamics of clean, layered superconductor/ferromagnet nanostructures using fully self consistent methods to solve the microscopic Bogoliubov-deGennes equations. From these self-consistent solutions the condensation free energies are obtained. The trilayer SFS junction is studied in particular detail: first order transitions between 0 and π states as a function of the temperature T are located by finding where the free energies of the two phases cross. The occurrence of these transitions is mapped as a function of the thickness d_F of the F layer and of the Fermi wavevector mismatch parameter Λ . Similar first order transitions are found for systems with a larger number of layers: examples are given in the 7 layer (3 junction) case. The latent heats associated with these phase transitions are evaluated and found to be experimentally accessible. The transition temperature to the normal state is calculated from the linearized Bogoliubov-deGennes equations and found to be in good agreement with experiment. Thus, the whole three dimensional phase diagram in T, d_F, Λ space can be found. The first order transitions are associated with dips in the transition temperature T_c to the non-superconducting state, which should facilitate locating them. Results are given also for the magnetic moment and the local density of states (DOS) at the first order transition.

PACS numbers: 74.45.+c, 74.25.Bt, 74.78.Fk

I. INTRODUCTION

The investigation of systems involving ferromagnet (F) and superconductor (S) junctions is an active component of superconductor-based spintronics¹ research. A broad array of interesting effects arises in S/F nanostructures, which opens doors for nanotechnologies and associated devices and applications that may offer benefits beyond current superconducting devices such as standard Josephson junctions. Advances in fabrication techniques permit growth of ferromagnet and superconductor layers in the form of junctions and heterostructures smooth up to the atomic scale.

The arrangement of consecutive F and S layers, as in SFS junctions, results in competition between magnetic and superconducting orderings. Superconducting correlations can leak into the ferromagnet while spin polarization can extend into the superconductor: these are the now well established S/F proximity effects.^{2,3} The phase coherence embodied in the superconducting correlations becomes modified in the F regions. The exchange energy in the ferromagnet shifts the kinetic energies of the quasiparticles constituting the Cooper pairs and subsequently a new superconducting state arises whereby the center of mass momentum of the pair is nonzero.⁴ This results in a spatially decaying pair amplitude that oscillates over a characteristic length scale much smaller than the superconducting coherence length. The modulating pair amplitude within the magnet indirectly links adjacent S layers, and thus proximity effects in F cause local oscillations in physically relevant single-particle quantities, including the magnetization^{5,6} and density of states^{7,8}

(DOS). Similarly, in the S material the magnet locally polarizes the superconductor, causing a monotonic decline in the pairing correlations near the interface over an extended region. The associated spin-split Andreev quasiparticle states also lead to interesting local behavior in the DOS and magnetic moment in the superconductor. The nontrivial behavior of the proximity effects in these structures plays a central role in the competition between the magnetic and superconducting order.

The modification of the superconducting phase coherence due to proximity effects in clean multilayers consisting of one or more successive SFS junctions is particularly striking. On the atomic level, the pair amplitude is a smoothly varying function of the spatial coordinates. Depending on the values of certain parameters (such as F layer width, d_F) the damped oscillatory pair amplitude in the F layer may arrange itself in such a manner that is energetically favorable for its sign to change from one of the S layers to the next, yielding a so-called π -junction, as first proposed long ago.⁹ If the pair amplitude does not change sign between S layers, it is an ordinary or 0-junction. There is a rich and broad parameter space that then enables a certain level of control over the competing magnetic and superconducting orderings, allowing one to increase or diminish the proximity effects that dominate the relative SFS coupling. The actual equilibrium state (0 or π) is dependent upon several variables, including predominantly the F region's material characteristics and the temperature, T , all of which ultimately determine the pair amplitude modulation in the magnet. A system comprised of a larger number of SFS sequences results in a greater number of possible 0 or π junction

combinations.

The transitions between 0 and π states can be explored through the signatures of a variety of physical parameters. Experimental study of this question has focused primarily on measurements of the critical current I_c ^{10–18} and, thermodynamically, on the critical temperature^{19–24} of the transition to the normal state, T_c . Evidence of $0 \leftrightarrow \pi$ transitions can be seen in the SFS Josephson coupling, which manifests itself in the vanishing of I_c , although higher order harmonics in the current-phase relationship can modify this.²⁵ Measurements^{19–24} as a function of d_F have shown that T_c , which is of course smaller than T_c^0 , the critical temperature for bulk S material, oscillates as a function of d_F , confirming theoretical predictions^{26,27} based upon the semi-classical Usadel equations. Intrinsically linked to this phenomenon are damped oscillations in I_c as a function of d_F and exchange energy in the clean²⁸ and dirty limits.^{29,30} These changes in the critical current have been experimentally confirmed^{10–18}. Of particular interest is Ref. 16, which demonstrates the robustness of $0 \leftrightarrow \pi$ transitions by providing evidence of switching in samples with interfaces that were not atomically smooth. Indeed, despite deviations as large as 0.6nm over 10% of a sample, clear evidence of switching was found. Near T_c , and in the diffusive limit, the theory was later extended to include arbitrary interface transparency.³⁰ Measurements of the superconducting phase¹³ have corroborated the π state in SFS junctions, and the predicted oscillations in several thermodynamic quantities have in many cases been found experimentally. Direct evidence of DOS oscillations was reported in a tunneling spectroscopy experiment,³¹ but not observed^{32,33} in other cases. Such studies give us the valuable insight that the oscillations are correlated with $\pi \leftrightarrow 0$ transitions. In this work, we show that there is indeed an intimate relation between the oscillations in T_c as a function of relevant parameters and the transitions from the π to the 0 state and we find good quantitative agreement with experimental data.

Since the possibility of having a particular junction configuration depends fundamentally on the intricate properties of the pair amplitude, the complicated and demanding task of calculating the pair potential, $\Delta(\mathbf{r})$, rigorously and self-consistently becomes absolutely necessary, particularly as the inhomogeneities occur on a microscopic scale. The first step in the self-consistency process often involves an assumed simple piecewise constant form for $\Delta(\mathbf{r})$, which is then iterated through the relevant equations until convergence is achieved. It is not justified to bypass the technical difficulties associated with self-consistency and to use only an assumed form for the pair potential. The final calculated $\Delta(\mathbf{r})$ often deviates significantly, even in overall symmetry, from the assumed form: the self-consistent $\Delta(\mathbf{r})$ has a complicated spatial behavior that can lead to stable states mixing 0 and π junction configurations.³⁴ A self-consistently calculated pair potential minimizes, at least locally, the free energy of the system. To determine whether the

calculated state is merely a local minimum of the free energy or the global one, the free energies from all possible self-consistent 0- and π -junction configurations must be compared with high precision. Recently developed numerical algorithms^{34,35} overcome the difficulties that arise in computing the small difference between much larger quantities and enable accurate computation of the differences in the values of the condensation free energy of different minima.

For clean SFS junctions, a relevant set of basic parameters to consider includes d_F , the exchange energy h_0 and T . As these parameters vary, the 0 or π -state free energies may cross at certain points in parameter space, yielding phase transitions. It has been shown³⁴ that at $T = 0$, transitions occur when varying h_0 , d_F and also the mismatch parameter Λ , defined as the ratio of Fermi energies in the F and S regions. This mismatch can induce a transition because at $\Lambda \approx 1$, when the Fermi wavevectors match, the layers couple more strongly, while at small Λ the coupling is effectively weaker. If the temperature varies it is also possible to have a first order transition between 0 and π junction states, as recently shown in both the clean,³⁵ and dirty³⁶ limits, and also predicted for short-period F/S superlattices.²⁶ The temperature has been shown to have a pronounced effect on the pair amplitude in the F region of F/S structures,³⁷ strongly diminishing its magnitude while maintaining its characteristic period of oscillation as T increases. This translates into weaker coupling between adjacent S layers. If the magnet width is such that the junction is near a $0 \leftrightarrow \pi$ transition point at $T = 0$, increasing the temperature can result in the critical current of the junction having a non-monotonic temperature dependence.²⁵ It has been argued³⁸ that the transition is discontinuous in uniform samples but rounded off in samples of variable thickness.³⁹ However, a transition can be observed¹⁶ in just a portion of samples with nonuniform thickness. These results indicate that the temperature can be used to switch between a 0 and a π state configuration. It is possible to locate regions of parameter space that give the desired transitions using the $T = 0$ results as guides, however the task is still significantly demanding. Such temperature transitions were found to occur in one-junction and 3-junction systems for moderate values of Λ .³⁵ Thus, a 1-junction system was found to have a $0 \rightarrow \pi$ first order transition as T was lowered, and a $\pi\pi\pi \rightarrow \pi 0\pi$ transition was found for a 3-junction system.³⁵ In each case, the free energies of a stable and a metastable state crossed at the transition temperature with differing derivatives, and therefore entropies. The existence of metastable states and an entropy discontinuity are hallmarks of first-order phase transitions. Moreover, the reported latent heats were reported to be within available experimental resolution. It is therefore desirable to systematically study the coexistence of metastable states and the nature of the transition in SFS and higher-order multilayer structures.

The main objective of this paper therefore, is to map out the regions of parameter space in which the different

junction states are stable, and to trace the locations of the phase transitions in systems with SFS junctions. An extensive sweep of the geometric and materials parameters including d_F , Λ , as well as T , is performed. To start with, it is important to know which d_F and Λ ranges allow more than one self-consistent state at $T = 0$. One can then check if a metastable state at low temperature becomes the equilibrium state at higher T . By using this procedure we obtain a complete phase diagram of an SFS junction within the relevant region of (T, Λ, d_F) space. To accomplish this, we use a method that can accommodate arbitrary values of the above parameters, without recourse to approximations. As discussed above, all calculations involving the pair potential must be performed using fully self-consistent algorithms, starting from the microscopic equations (Bogoliubov-deGennes (BdG)). The need for a fully microscopic theory arises because the characteristic period of the pair potential oscillations approaches the atomic scale. For the nanoscale interlayer widths considered here, geometrical oscillations decisively influence the final results.

We present in Sec. II the microscopic equations and the associated notation relevant for systems containing SFS junctions. We review the numerical procedures involved in calculating the self-consistent pair potential and quasiparticle spectra, and the method used to calculate the primary thermodynamic quantity, the condensation free energy, $\Delta\mathcal{F}(T)$, from the self-consistent spectrum and pair potential. We also outline a semi-analytic method to calculate T_c through the linearized BdG equations. In Sec. III, we show that first order transitions with measurable latent heat can occur between states containing different numbers of 0 and π junctions as the temperature changes. For SFS junctions the transitions we find are from the π to the 0 state as T increases, as found in experiment,¹⁶ and occur predominantly in re-

gions where T_c is low. Using the T_c calculated from the linearized theory and the $0 \leftrightarrow \pi$ phase transitions, we obtain the full phase diagram in an extended region of parameter space spanned by T , d_F , and Λ . We compare our calculated oscillations in T_c as a function of d_F with reported Nb/Co experimental data²⁰ and find good agreement.

II. METHODS

The systems that we study consist of slabs of clean superconductor (S) material separated by ferromagnetic (F) layers. We will emphasize trilayers consisting of one SFS junction and, as a sample of what can generally occur in multilayers, present also results for seven layer systems consisting of three SFS junctions. The thickness of the S layers in an SFS junction is denoted by d_S , and that of the F layers by d_F . The seven layer system consists of three SFS junctions stacked together, so that the thickness of the two inner S layers is $2d_S$. We assume that the layers are semi-infinite in the directions perpendicular to the interfaces (the $x - y$ directions) and that the interfaces are sharp. The spatial inhomogeneity is confined to the z direction, allowing us to model the system as quasi one dimensional. We assume parabolic bands, thus in the transverse direction $\epsilon_\perp = k_\perp^2/2m$, where k_\perp is the wavevector in the transverse direction and ϵ_\perp is the energy corresponding to the $x - y$ variables.

We use the microscopic Bogoliubov-deGennes⁴⁰ equations to study this inhomogeneous system. Given a pair potential (order parameter) $\Delta(z)$ that is to be determined self consistently, the spin-up quasi-particle ($u_n^\uparrow(z)$) and spin-down quasi-hole ($v_n^\downarrow(z)$) amplitudes obey the BdG equations in the following form:

$$\begin{pmatrix} H - h(z) & \Delta(z) \\ \Delta(z) & -(H + h(z)) \end{pmatrix} \begin{pmatrix} u_n^\uparrow(z) \\ v_n^\downarrow(z) \end{pmatrix} = \epsilon_n \begin{pmatrix} u_n^\uparrow(z) \\ v_n^\downarrow(z) \end{pmatrix}. \quad (2.1)$$

Here, $H = p_z^2/2m - E_F(z) + \epsilon_\perp$ is a single-particle Hamiltonian where $p_z^2/2m + \epsilon_\perp$ is the kinetic energy term. The continuous variable ϵ_\perp is decoupled from the z direction but of course it affects the eigenvalues ϵ_n . We describe the magnetism by an exchange field $h(z)$ which takes the value h_0 in the F material and vanishes in S. Within the superconducting layers, $E_F(z)$ is equal to E_{FS} , the Fermi energy of the S layers measured from the bottom of the band, while in the ferromagnet we have $E_F(z) = E_{FM}$ so that in the F regions the up and down band widths are $E_{F\uparrow} = E_{FM} + h_0$ and $E_{F\downarrow} = E_{FM} - h_0$ respectively. In the seven layer case we assume parallel orientation of the magnetization in all F layers. One should not as-

sume that $E_{FM} = E_{FS}$ and we therefore introduce the dimensionless Fermi wavevector mismatch parameter Λ by $E_{FM} \equiv \Lambda E_{FS}$. Usually, one has $\Lambda < 1$. It is also convenient to introduce the dimensionless magnetic strength variable I by $h_0 \equiv E_{FM}I$. The $I = 1$ limit corresponds to the ‘‘half-metallic’’ case. We neglect interfacial scattering. The amplitudes $u_n^\uparrow(z)$ and $v_n^\downarrow(z)$ can be written down from symmetry relations.⁴⁰

The required self-consistency condition for the pair potential $\Delta(z)$ is:

$$\Delta(z) = \frac{g(z)}{2} \sum_n' (u_n^\uparrow(z)v_n^\downarrow(z) + u_n^\downarrow(z)v_n^\uparrow(z)) \tanh\left(\frac{\epsilon_n}{2T}\right) \quad (2.2)$$

where here and below the prime indicates a summation over states for which $|\epsilon_n| \leq \omega_D$, where ω_D is the usual cutoff “Debye” energy and it is understood that the index n includes k_\perp as well as the longitudinal variables. The BCS coupling $g(z)$ is taken to be a constant g in the superconductor and zero in the ferromagnet.

A. Self-Consistent Solutions

Equations (2.1) and (2.2) comprise a non-linear set of equations. Exact solutions to this set must be computed in a self-consistent manner. We follow the procedure^{6,7,35} used in previous work; we omit the repetition of the technical details. We begin with an assumed form for $\Delta(z)$, either from a prior calculation with similar parameters or an *a priori* guess (usually a stepwise function), and then numerically solve Eq. (2.1) for every value of ϵ_\perp in the appropriate range to compute $u_n^\uparrow(z)$, $v_n^\downarrow(z)$, and ϵ_n . An expansion of all quantities in terms of sine waves is used⁷ to carry out the solution. The required matrix elements are given, for our geometries, in Ref. 6. This resulting energy spectrum and quasiparticle amplitudes are used in Eq. (2.2) to compute a new $\Delta(z)$. We then feed this new $\Delta(z)$ back into Eqs. (2.1) and repeat this process until

the fractional difference between the average of successive solutions for $\Delta(z)$ is less than a threshold value that we take to be 10^{-5} . Solutions obtained in this way are exact up to the chosen numerical precision.

The self-consistent solution for a trilayer SFS junction can be of the π or the 0 type, with the pair potential either changing or not changing sign across the F layer, respectively. More complicated situations can occur in multilayers: for a three junction system one can encounter four symmetric states (000, 0 π 0, π 0 π , $\pi\pi\pi$, with each symbol corresponding to the state of each junction). When, for a given temperature and set of geometrical and material parameters such as I , d_F , and Λ , several^{6,7,35} different self-consistent solutions, that is, local minima in the free energy, exist, the stable state must be determined by comparing the condensation free energies of the competing self-consistent states. As discussed in Sec. I, when the equilibrium state changes as a function of temperature³⁵ a first order phase transition can occur, with a corresponding latent heat. One of the chief goals of this paper is to study an extended region of parameter space, locating where such transitions exist and then mapping out the corresponding phase diagram.

To evaluate the free energy, \mathcal{F} , of the self-consistent states we use the formula from Ref. 41:

$$\mathcal{F}(T) = -2T \sum_n' \ln \left[2 \cosh \left(\frac{\epsilon_n}{2T} \right) \right] + \frac{1}{d} \int_0^d \frac{\Delta^2(z)}{g(z)} dz, \quad (2.3)$$

where d is the total thickness of the system in the z -direction. In this expression, only the energy eigenvalues appear explicitly, the eigenfunctions appearing only indirectly through the self-consistent $\Delta(z)$. It is equivalent to several other expressions found in the literature which contain the quasi-particle amplitudes explicitly, but it is computationally much more convenient.

The condensation free energy is defined as $\Delta\mathcal{F}(T) \equiv \mathcal{F}_S - \mathcal{F}_N$, where \mathcal{F}_S is the free energy of the superconducting state and \mathcal{F}_N that of the non-superconducting system. We compute \mathcal{F}_N by setting $\Delta = 0$ in equations (2.1) and (2.3). Calculating $\Delta\mathcal{F}(T)$ is a significant numerical challenge: recall that in a bulk superconductor⁴² $\Delta\mathcal{F}(0) = -(1/2)N(0)\Delta_0^2$, where $N(0)$ is the usual density of states and Δ_0 is the order parameter for the bulk superconductor at $T = 0$, which is several orders of magnitude smaller than $\mathcal{F}_N \propto N(0)\omega_D^2$. Hence, to obtain $\Delta\mathcal{F}$ we must subtract two numerically obtained large quantities in order to extract a difference several orders of magnitude smaller than the terms subtracted. Furthermore, as we shall see, the difference in condensation free energies of competing self-consistent states (when they occur) is only a small fraction of the condensation free energy of each of them. To obtain sufficiently accurate values

of $\Delta\mathcal{F}$ requires therefore a very high degree of precision in calculating \mathcal{F}_S and \mathcal{F}_N so that we can distinguish the relatively small differences between competing states to locate phase transitions. This situation is made more challenging by the need to calculate derivatives of $\Delta\mathcal{F}$ to obtain thermodynamic functions and latent heats.

B. Calculation of T_c : Linearized Solution

While the transition temperature T_c from the non-superconducting to the superconducting state can be numerically calculated as the temperature at which $\Delta\mathcal{F}$ vanishes, it is much easier to evaluate T_c by treating $\Delta(z)$ as a small parameter and linearizing the equations. In this way the calculation is nearly entirely analytic. The amplitudes are written as $u_n^\uparrow(z) = u_n^0(z) + u_n^1(z)$ and $v_n^\downarrow(z) = v_n^0(z) + v_n^1(z)$ (we have dropped the spin indices for simplicity). The $u_n^0(z)$ and $v_n^0(z)$ terms are computed from the zeroth order equation, which is obtained by setting $\Delta(z) = 0$ in Eq. (2.1). The form of the zeroth order equation implies that $u_n^0(z)$ and $v_n^0(z)$ are completely decoupled and have distinct energy spectra, denoted by ϵ_n^p and ϵ_n^h respectively. Proceeding to calcu-

late the lowest order corrections, we incorporate quasiparticle coupling through the pair potential matrix. One can then obtain $u'_n(z)$ and $v'_n(z)$ from textbook perturbation formulas. The intermediate sums are in principle over the entire zeroth order spectrum. but as a practical matter it is enough to include in these sums energies ϵ_n^p and ϵ_n^h within a few ω_D of the Fermi level.

We then expand the quasiparticle amplitudes and their first order corrections in a sine wave basis $\phi_q(z)$, e.g. $u_n^0(z) = \sum_q^N u_{qn} \phi_q(z)$ and $v'_n(z) = \sum_q^N v'_{qn} \phi_q(z)$, where $\phi_q(z) = \sqrt{2/d} \sin(k_q z)$, with $k_q = q\pi/d$. The range of the sums over k_q is formally infinite, but again it is only necessary to sum up to a wavenumber k_N with an

associated energy a few ω_D from E_F . Inserting these expansions into Eq. (2.2) gives the lowest order correction to $\Delta(z)$, which we then expand in the $\phi_q(z)$ basis. Upon taking into account the orthogonality of the basis functions, the expanded Eq. (2.2) is then transformed into the matrix equation

$$\Delta_l = \sum_k J_{lk} \Delta_k, \quad (2.4)$$

where the Δ_k are the expansion coefficients of $\Delta(z)$ in terms of $\phi_k(z)$. One finds after straightforward algebra:

$$J_{lk} = \frac{gN(0)}{4\pi} \int d\epsilon_\perp \sum_n' \left\{ \sum_m \sum_{pq}^N u_{pn}^0 v_{qm}^0 K_{pql} \frac{\sum_{ij}^N v_{im}^0 u_{jn}^0 K_{ijk}}{\epsilon_n^p - \epsilon_m^h} \tanh\left(\frac{\epsilon_n^p}{2T}\right) + \sum_m \sum_{pq}^N v_{pn}^0 u_{qm}^0 K_{pql} \frac{\sum_{ij}^N u_{im}^0 v_{jn}^0 K_{ijk}}{\epsilon_n^h - \epsilon_m^p} \tanh\left(\frac{\epsilon_n^h}{2T}\right) \right\}. \quad (2.5)$$

Here we have used $gK_{ijk} = \int_0^d g(z)\phi_i(z)\phi_j(z)\phi_k(z)dz$. The integral over ϵ_\perp reflects the dependence of the zeroth order quasiparticle amplitudes and energies on ϵ_\perp , and the sum over n is here only over longitudinal quantum numbers with the prime denoting the limitation indicated below Eq. (2.2) on the energies ϵ_n^p and ϵ_n^h .

The transition temperature can then be found, in analogy with standard procedures,^{43,44} by treating Eq. (2.4) as an eigenvalue equation for the matrix J_{lk} . At the transition temperature T_c the largest eigenvalue is unity, while if $T > T_c$ all eigenvalues are less than unity. Unlike the free energy method described in subsection II A, this procedure does not require an iterative process and only the last step (finding the eigenvalue) must in practice be performed numerically. Therefore this method is much more efficient, and it also provides a check on the numerics of our free energy.

C. Other quantities

From the self-consistent amplitudes and an energy spectrum we can also calculate other quantities of interest such as the density of states (DOS) and the magnetization. The local density of states is

$$N(z, \epsilon) = - \sum_\sigma \sum_n \left[[u_n^\sigma(z)]^2 f'(\epsilon - \epsilon_n) + [v_n^\sigma(z)]^2 f'(\epsilon + \epsilon_n) \right] \quad (2.6)$$

where σ denotes spin and $f'(\epsilon)$ is the first derivative of the Fermi function. One can also omit the sum over σ and obtain the spin dependent DOS.

Similarly, we have the average number density for each spin subband,

$$\langle n_\sigma(z) \rangle = \sum_n \left\{ [u_n^\sigma(z)]^2 f(\epsilon_n) + [v_n^\sigma(z)]^2 [1 - f(\epsilon_n)] \right\}. \quad (2.7)$$

This leads to the dimensionless magnetization, $M(z)$,

$$M(z) = \frac{\langle n_\uparrow(z) \rangle - \langle n_\downarrow(z) \rangle}{\langle n_\uparrow(z) \rangle + \langle n_\downarrow(z) \rangle}, \quad (2.8)$$

which reduces to $M(z) = \frac{[(1+I)^{3/2} - (1-I)^{3/2}]}{[(1+I)^{3/2} + (1-I)^{3/2}]}$ for bulk F material, within our assumptions. This expression is in numerical agreement with our results from Eq. (2.8) in sufficiently thick F layers.

III. RESULTS

In this section we present and discuss our results. As explained above, trilayers consisting of one SFS junction will be emphasized but results for seven layer systems comprised of three stacked SFS junctions will also be given in order to show that the single junction results can indeed be generalized to multilayer samples. We will first discuss the results for the thermodynamics and the phase transitions that ensue. This will include a detailed discussion of the phase diagram for the SFS trilayer in the most interesting region of the three dimensional space spanned by T , Λ and the F layer thickness. A discussion of the properties of the transition temperature T_c as a function of d_F and a comparison with experiment follow.

We will also discuss other quantities of interest, such as the pair amplitude, the density of states, and the magnetization.

A. Parameters and Units

The results presented below will be given in terms of convenient dimensionless quantities. We measure all the lengths in units of k_{FS}^{-1} , the Fermi wavevector in S. We fix $D_S \equiv k_{FS}d_S = 100$. We have taken the BCS coherence length ξ_0 equal to d_S . For d_S of order of or larger than ξ_0 , results are only weakly dependent on d_S , hence our results are applicable to a very wide range of values of this variable, provided d_S is not too small. The dimensionless thickness $D_F \equiv k_{FS}d_F$ of the ferromagnetic layers will be varied over the range of interest, which corresponds to relatively small values, since at large ones the F/S proximity effects are negligible. Similarly, we introduce the notation $Z \equiv k_{FS}z$. The magnetic strength parameter is taken to be $I = 0.2$ unless otherwise noted. The effects of varying I are physically similar to those of varying D_F since the pair amplitude oscillations in F are governed⁴ by the difference $(k_\uparrow - k_\downarrow)d_F$ between Fermi wavevectors in the spin bands in F. The Fermi wavevector mismatch parameter, Λ , to which results are quite sensitive, is varied over the experimentally relevant range $0.1 \leq \Lambda \leq 1$. The temperature is measured in units of T_c^0 , the critical temperature of a bulk sample of the material S. We choose $\omega_D/E_{FS} = 0.02$; the dimensionless quantities calculated are not sensitive to this choice. Condensation free energies will be given in units of $N(0)\Delta_0^2$, twice the absolute value of the condensation free energy of a bulk superconducting sample of the same total thickness at $T = 0$. A dimensionless measure of the latent heats will be given by dividing the corresponding entropy discontinuities by $C_n(T_c^0)$, the specific heat of a sample of the same overall thickness but consisting exclusively of the S material in its normal metal state at T_c^0 .

We performed several checks of our numerical methods. We verified that the temperature at which the self-consistent condensation free energy goes to zero is in each case the same as the transition temperature obtained from the linearized solution to the BdG equations. For a sample with $d_S \gg \xi_0$ and $d_F = 0$, we quantitatively recovered the well established results⁴² for the thermodynamics, including the second order phase transition at T_c^0 and the associated specific heat discontinuity. Furthermore, the spatially averaged DOS computed numerically for this system shows a well defined gap at energies within Δ_0 of E_F and the characteristic divergence at $E_F \pm \Delta_0$. This test is very severe since our numerical method must necessarily be more accurate for smaller systems, where fewer variables are required. Thus the ability of our numerical procedures to handle the relatively large systems (over six superconducting correlation lengths thick) considered here is verified. The low temperature limit was extensively checked in Ref. 6, and it was also previously

verified⁷ that our methods give the correct thickness dependence of $\Delta(z)$ for a superconducting slab as found in the literature⁴⁵.

B. Free energy

The basic quantity that determines the phase transitions and the entire thermodynamics is the condensation free energy, $\Delta\mathcal{F}(T)$. We will therefore begin our exposition by describing some of our results for $\Delta\mathcal{F}(T)$ at a few parameter values representative of the regions where the phase transition behavior is richest.

We begin with Fig. 1 which shows, for an SFS trilayer, the self-consistent condensation free energy $\Delta\mathcal{F}(T)$ plotted versus reduced temperature T/T_c^0 . Data points were obtained at $T/T_c^0 = 0.01$ intervals. The values of D_F and Λ for which results are shown were chosen to be such that, at $T = 0$, self-consistent solutions of both the 0 and the π states are found to exist. In each panel, the free energies of the two competing states are shown. The thermodynamically stable state is of course the one with the lower free energy. The slope of $\Delta\mathcal{F}(T)$ approaches zero as $T \rightarrow 0$, which indicates that the calculated entropy vanishes at $T = 0$ as required by the third law of thermodynamics. The slope also approaches zero as $\Delta\mathcal{F}(T) \rightarrow 0$, indicating that the transition to the normal state is of second order, without latent heat. The temperature at which this second order phase transition occurs, T_c , is the temperature at which the lower $\Delta\mathcal{F}(T)$ vanishes. The T_c found this way agrees with the independently calculated T_c using the linearized BdG equations. The inherent finite-size and proximity effects cause T_c to be considerably smaller than T_c^0 in all cases.

Two outstanding features of the results shown in this figure are the existence of a metastable state at all temperatures from zero up to T_c and a first order phase transition at an intermediate temperature: the free energies of the two competing states cross at $T = T_x$. In all cases shown the π state is stable below T_x and the 0 state is stable above. The position of T_x is marked by the vertical arrow in each panel. The value of T_x changes smoothly as D_F or Λ are changed. One can see by comparing top and bottom panels how T_x changes with D_F at constant Λ .

In Fig. 1 one can see the difference in slope between the stable state and the metastable state at T_x , particularly apparent in the right panels. The existence of a metastable state and the discontinuity in the slope of the free energy of the stable state (i.e., the entropy) at T_x indicate the existence of a first order phase transition with an associated latent heat. That any such transition should be first order can also be expected from the change of symmetry of the pair amplitude. For a range of parameter values including those shown in this figure, the phase transition behavior is exceptionally rich. In many other regions of Λ and D_F parameter space the behavior is simpler: in some there is only one self con-

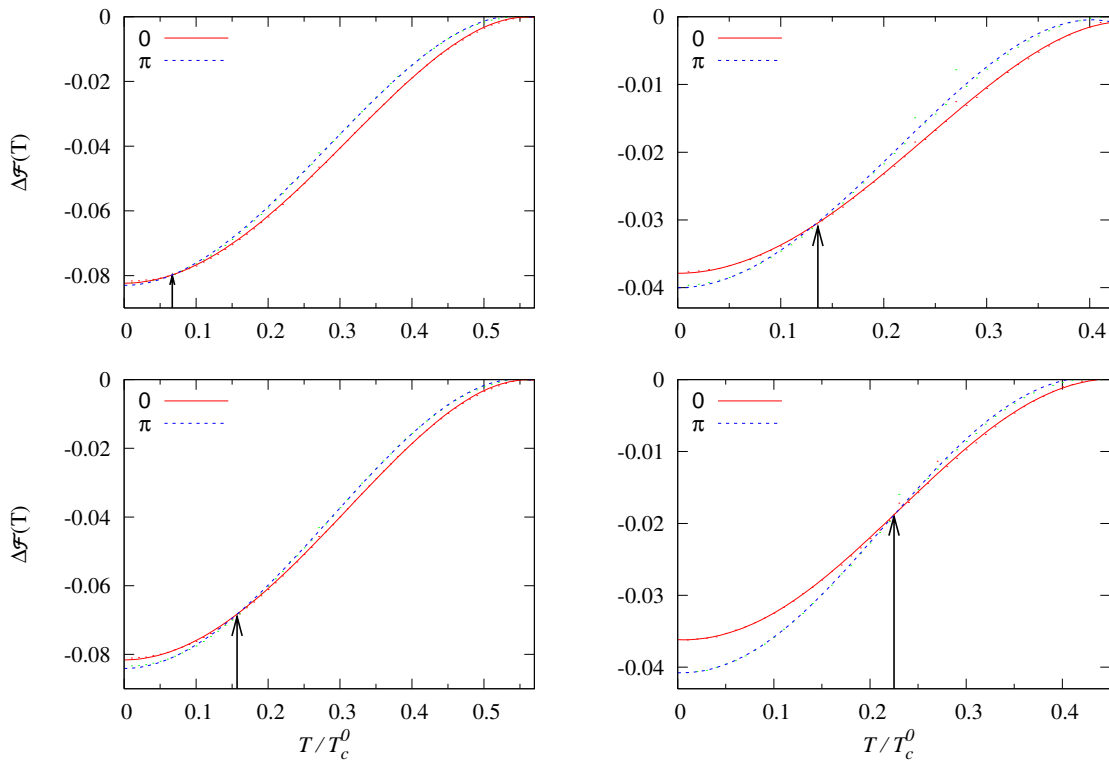


FIG. 1: (Color online) Results for the normalized (see text) condensation free energy $\Delta\mathcal{F}(T)$ vs. temperature for a 3 layer SFS junction. The different curves are labeled in the legends. In all cases shown, upon increasing T a π to 0 transition occurs at temperature T_x , indicated by the arrows. The top left panel shows results for $\Lambda = 0.550$ and $D_F = 7.0$, resulting in $T_x/T_c^0 = 0.07$. Bottom left: $\Lambda = 0.550$ and $D_F = 7.1$, with $T_x/T_c^0 = 0.16$. Top right: $\Lambda = 0.650$ and $D_F = 5.8$, with $T_x/T_c^0 = 0.13$. Bottom right: $\Lambda = 0.650$ and $D_F = 5.9$, resulting in $T_x/T_c^0 = 0.23$.

sistent solution to the BdG equations at $T = 0$, while for other ranges of Λ and D_F a metastable state is found at low temperature but it never becomes the stable state as T increases. It is only in some regions of parameter space that $0 \leftrightarrow \pi$ transitions occur as a function of T . This question will be discussed in more detail below.

Examples of similar results for the 7 layer case are shown in Fig. 2. These are all at $\Lambda = 0.55$, for several values of D_F . In all cases shown at least two of the four possible metastable states mentioned above exist over the entire temperature range. The states shown in each panel are the two lowest in free energy. In some cases additional states exist but with higher free energy throughout: any such states are omitted from the plots. The three panels illustrate three different types of phase transitions as T increases: $\pi 0 \pi \rightarrow \pi \pi \pi$ (one junction flipping $0 \rightarrow \pi$), $0 \pi 0 \rightarrow \pi 0 \pi$ (three flips), and $0 \pi 0 \rightarrow 0 0 0$ (one flip, $\pi \rightarrow 0$). Each of these persists over a range of D_F . The results show all of the same qualitative features as the three layer case: the slope of $\Delta\mathcal{F}(T)$ approaches zero as $T \rightarrow 0$ and as $\Delta\mathcal{F}(T) \rightarrow 0$. There is again a change in the slope of the stable state at T_x which shows that the transition is also of first order in multi-junction cases. We will show that the latent heats are of the same magnitude as or

larger than in the 3 layer case. There is an important quantitative difference: T_x varies more slowly with D_F or Λ and therefore the range of parameter values for which such transitions are found is wider. One can expect then, that in higher order multilayers these phenomena will be even more general.

C. Thermodynamic functions

From the free energy one can obtain the entire thermodynamics. Figure 3 shows some of the thermodynamic functions that can be obtained from the results shown in Fig. 1. Results are shown for two quantities: the dimensionless condensation entropy $S(T)$, defined as the negative derivative of $\Delta\mathcal{F}(T)$ with respect to the reduced temperature T/T_c^0 , and the dimensionless condensation energy $U(T)$ defined as $U(T) \equiv \Delta\mathcal{F}(T) + (T/T_c^0)S(T)$. Results are shown for both the stable and the metastable states as a function of reduced temperature. One sees that $S \rightarrow 0$ smoothly as $T \rightarrow 0$ and $T \rightarrow T_c$ in each case, which is an important check on the computation. The condensation entropy, energy, and free energy all vanish at T_c . In each panel a bold vertical line indicates T_x .

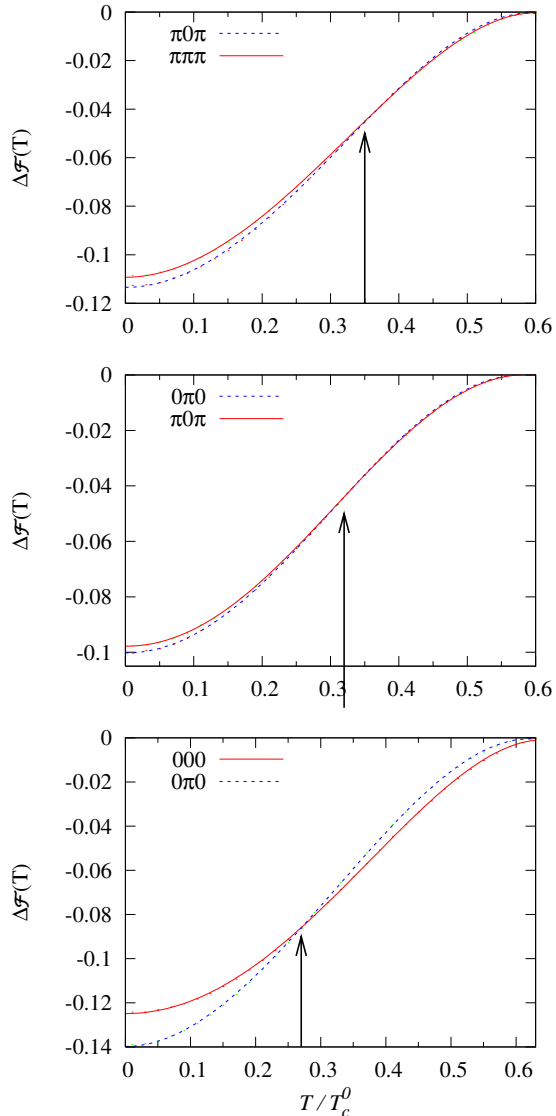


FIG. 2: (Color online) Results for $\Delta\mathcal{F}(T)$ vs. reduced temperature (as in Fig. 1) for a 7 layer system. T_x is indicated by the arrows. The different curves are labeled in the legends. The top panel shows a $\pi 0\pi \rightarrow \pi\pi\pi$ transition for $\Lambda = 0.55$ and $D_F = 9.1$. The transition occurs at $T_x/T_c^0 = 0.37$. The middle panel shows a $0\pi 0 \rightarrow \pi 0\pi$ transition for $\Lambda = 0.55$ and $D_F = 7.9$, at $T_x/T_c^0 = 0.33$. The bottom panel shows a more pronounced $0\pi 0 \rightarrow 000$ transition for $\Lambda = 0.55$ and $D_F = 4.75$, with $T_x/T_c^0 = 0.27$.

The free energy crossings correspond neither to crossings in $S(T)$ nor to crossings in $U(T)$. The former follows from the phase transitions being of first order with an associated discontinuity in the entropy. Both the energy and the entropy, therefore, play important roles in the phase transition. The specific heat is not shown but can be calculated by taking a further derivative.

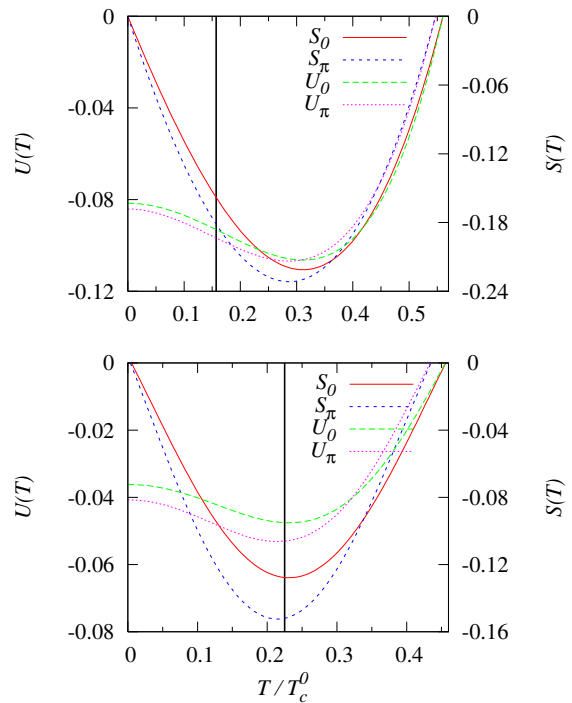


FIG. 3: (Color online) Thermodynamic functions of an SFS trilayer. The top and bottom panels show the condensation energy and entropy (in dimensionless form, see text) for the two sets of parameter values used, respectively, in the left and right bottom panels of Fig. 1. The meaning of different curves is indicated in the legend. The location of the first order transition is marked by the bold vertical line.

Examples of the thermodynamic functions for the 7 layer system are shown in Fig. 4. The 3 junction case is again qualitatively much like the one junction case. The entropy, energy, and free energy all go to zero in the appropriate limits. There is no crossing in energy or entropy at T_x , indicating the important interplay between energy and entropy. The discontinuity in the entropy at T_x also reflects a latent heat, comparable to or larger than that in the one junction case.

The behavior of the Cooper pair amplitude at the first order transition is illuminating. Figure 5 shows, for the SFS trilayer at $T = T_x$, the pair amplitude (defined in the usual way as the average of spin up and down creation operators) normalized to Δ_0/g , its value in bulk S material at $T = 0$. Results are given versus dimensionless position Z . The F region is in the middle, set off by vertical dotted lines, and only small portions of the S regions are shown. The two cases shown correspond to the two bottom panels in Fig. 1. The absolute value of the pair amplitude is discontinuous at T_x : in both plots it is slightly larger for the 0 state. We recall that for a bulk superconductor at $T = 0$, the free energy

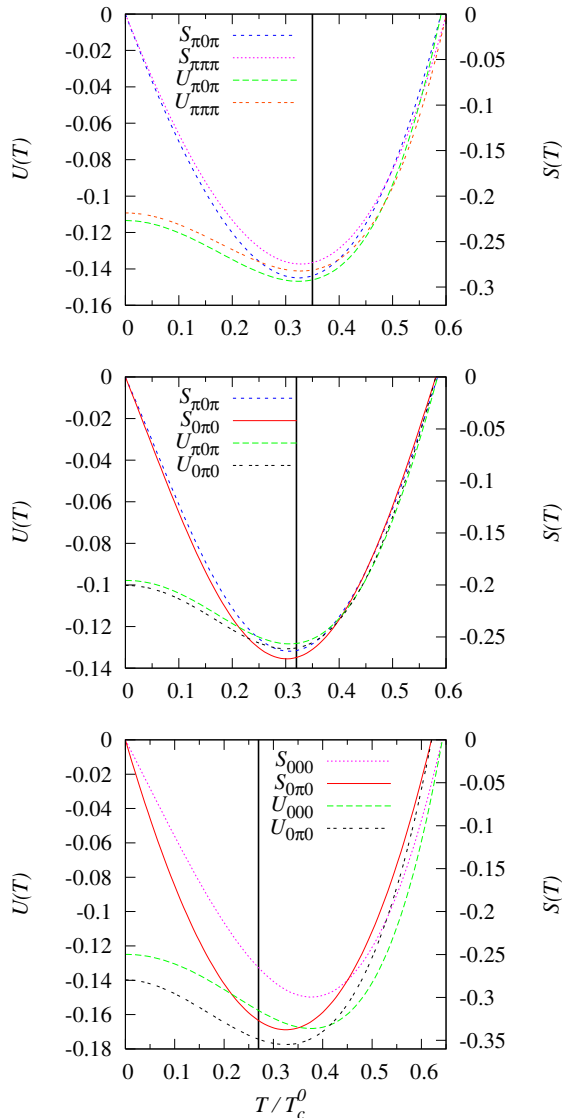


FIG. 4: (Color online) Thermodynamic functions of a 7 layer system. The panels show the condensation energy and entropy (as in Fig. 3) for the parameter sets used in Fig. 2. The different curves are labeled in the legend, extending the notation introduced in Fig. 3. The location of T_x is marked by the bold vertical line.

is proportional to the average value of the squared pair potential,⁴² and this is also⁶ approximately the case at $T = 0$ for SFS layered systems when $d_F \ll d_S \ll \xi_0$. Even in the bulk system, however, such a relationship is not valid⁴⁶ at finite temperature. It is therefore unreasonable to expect this proportionality in the layered case and indeed it does not occur: the pair amplitudes do not change continuously at T_x . We conclude that the phase transitions are not driven by the pair amplitude.

The pair amplitude for the three junction system dis-

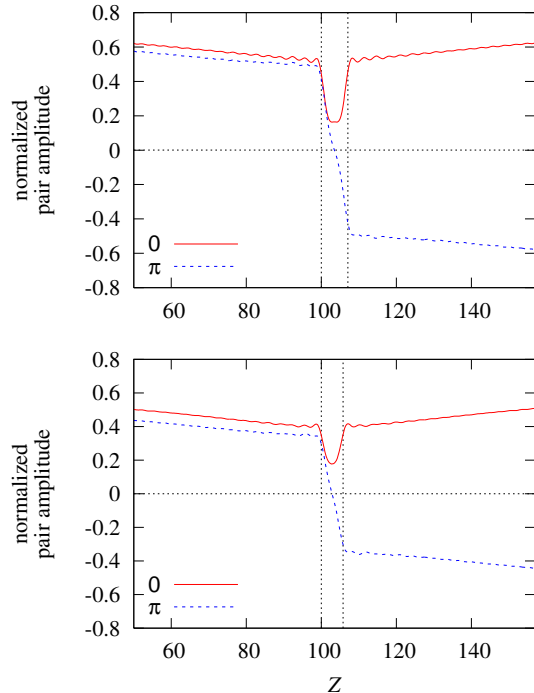


FIG. 5: (Color online) The normalized (see text) pair amplitude for the 0 and π states of the SFS trilayer, at the crossing point T_x , as a function of position $Z \equiv k_{FS}z$. Only the middle portion of the sample is shown. The F layer is delimited by the vertical dotted lines. Results are presented (top and bottom panels) for the two sets of parameter values used, respectively, in the left and right bottom panels of Fig. 1.

plays properties that are very similar to those of a single junction. A representative example, corresponding to $\Lambda = 0.55$ and $D_F = 4.75$, is shown in Fig. 6. The absolute value of the amplitude is again discontinuous at T_x . It is very important that the 7 layer and the 3 layer systems have qualitatively similar properties, as this shows that the phenomena we discuss are very general. At the same time, in the 7 layer case there is a greater number of possible transitions and the regions of parameter space in which they occur as a function of T are wider, indicating that such phenomena can be more readily found in more complicated systems. We can make qualitative predictions for the 7 layer system based on our quantitative (but computationally less demanding) calculations for the 3 layer system. Thus, the properties of a single junction system can be generalized to systems with many junctions.

D. Latent heats

The signature of a first order phase transition is its latent heat. In Fig. 7 we show results for the dimensionless latent heat L , defined as the difference between

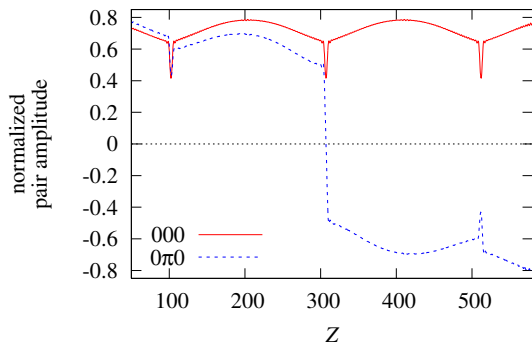


FIG. 6: (Color online) The dimensionless (see text) pair amplitude for the $0\pi 0$ and 000 states of the 7 layer system for $\Lambda = 0.55$ and $D_F = 4.75$ at the crossing point T_x as a function of position Z . This is the parameter set used in the bottom panel of Fig. 2.

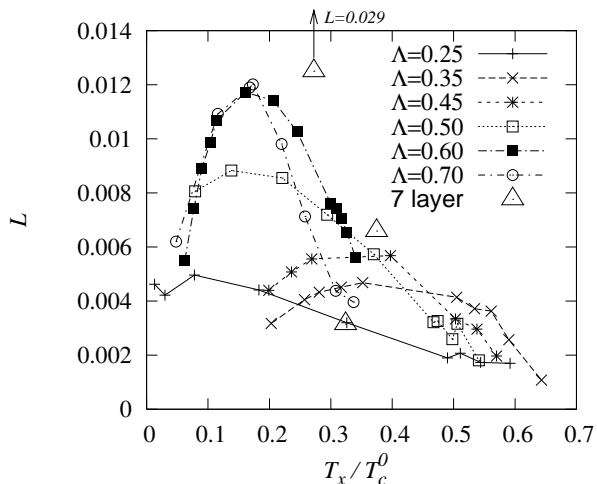


FIG. 7: Latent heats. L is the entropy discontinuity in units of $C_n(T_c^0)$ (see text). It is plotted against the reduced temperature of the first order phase transition. The symbols joined by lines are for an SFS trilayer: the value of T_x is changed along the horizontal axis by varying D_F , and from curve to curve by varying Λ (see legend). The triangles are for the 7 layer system cases shown in Fig. 2. The vertical arrow attached to the topmost triangle indicates that it corresponds to a value $L = 0.029$ (off the scale).

the entropy of the stable states just above and just below T_x divided by $C_n(T_c^0)$, the specific heat of a normal bulk sample of S material at $T = T_c^0$. This is appropriate because $C_n(T)$ is equal to the entropy in the free electron model. Results are plotted as a function of T_x . Most of the results shown are for a single junction: in that case the crossing temperature is varied by changing D_F for several different values of Λ , as indicated by the symbols connected by straight segments. The three data points indicated by the isolated triangles correspond to the three transitions shown in Fig. 2 for the 7 layer system. One of them corresponds to a value larger, by over

a factor of two, than the upper end of the scale.

The latent heats vanish as T_x approaches 0 or T_c , consistent with the smaller condensation entropy of each state in those limits. However, whenever T_x does not approach these limits the latent heat can exceed 1% of $C_n(T_c^0)$ for one junction, and even more for the three junction system. Since we give L in units of C_n , which is an extensive property, it should be easier to observe these latent heats in larger systems. A value of $L \approx 0.01$ would correspond to picojoules in actual samples of relatively small size.¹⁰ Such latent heats can be readily observed via standard techniques used to measure specific and latent heats in films.⁴⁷ Even smaller specific heats can be measured using multiple samples: attojoule level results have been reported⁴⁸ in electronic systems. We see therefore that whenever a first order transition occurs, the associated latent heat is observable.

E. Phase diagram

We have seen that in an SFS trilayer there are two kinds of phase transitions. First, there are second order phase transitions from the normal state to a superconducting state of either the 0 or the π kind. There are also, at certain ranges of the relevant parameters, first order transitions between the 0 and π superconducting states. As a practical matter, observability of the latter transitions through thermodynamic measurements requires an appreciable difference in condensation energies between the two states. This difference is an oscillatory function of D_F at constant Λ and I (see e.g. figure 3 of Ref. 6) with the oscillations becoming damped at large D_F , since then, at any $I > 0$ the proximity effects are reduced and the 0 and π states are degenerate. Hence the most important regions theoretically and experimentally are at relatively small values of D_F . As to Λ , the entire region $\Lambda < 1$ is relevant.

Therefore, we have mapped out the entire phase diagram of an SFS trilayer in this most relevant region of (T, Λ, D_F) space in Fig. 8. As explained above, varying I is equivalent to varying D_F , so we use D_F as the more experimentally relevant parameter. We show two views of the phase diagram to aid in the visualization of this three dimensional figure. There are three regions in this diagram, each representing one of the three possible states: 0 state, π state, and normal (not superconducting) state. The crossings T_x are calculated from the free energies, and T_c through the linearization method.

The top sheet shows the superconductor/normal metal transition. As $D_F \rightarrow 0$, T_c/T_c^0 approaches unity for all Λ . At small Λ the sheet also flattens, since then the Fermi level of the ferromagnet is small compared to E_{FS} so that there is little interaction between the Cooper pairs and the ferromagnet. The finite temperature T_x transitions between 0 and π regions are located at the sheet or “wall” that goes from the $T = 0$ plane to the T_c sheet, separating the 0 from the π state regions. This wall is of course not

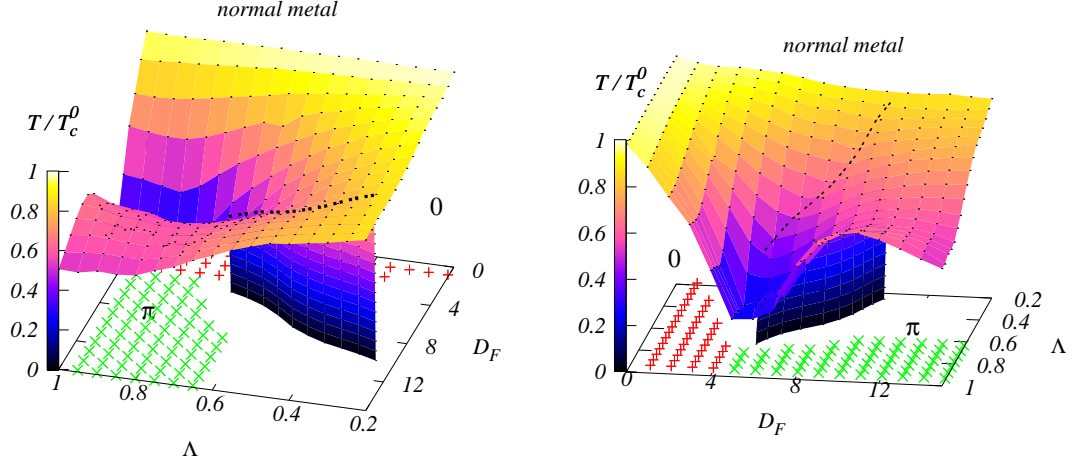


FIG. 8: (Color online) The (Λ, D_F, T) phase diagram for the 3 layer system. The two panels show different views of the same plot. There are three regions: in those labeled 0 and π , the 0 and π states are, respectively, the equilibrium state, while *normal metal* indicates where the sample is nonsuperconducting. The top surface separates non-superconducting and superconducting regions. The fairly vertical sheet marks the temperature transitions between 0 and π states. The intersection of the 0 – π and the T_c boundaries is marked by a dotted line. The portion of the $T = 0$ plane marked by \times symbols is the range of (Λ, D_F) for which only the π state exists for all T : there is no metastable state of the 0 type. Likewise, in the region marked by + symbols only the 0 state exists. In the portion left blank, solutions of both kinds are possible.

completely vertical: its deviation from verticality is what causes first order phase transitions as a function of T . On the smaller D_F end, this wall ends because one of the two states becomes unstable: a region of parameter space is entered where only one self consistent solution exists at any temperature. Coincident with this, as one can see more clearly in the right panel, T_c is sharply reduced: in other words, the condensation energies of both states rise towards zero, with one actually vanishing. Near this region T_c has always a sharp dip. As one proceeds towards the opposite end of the wall, at larger values of D_F , T_c increases and the wall becomes steeper, until it eventually becomes vertical. Beyond that, no transition occurs as a function of T : the stable state is the same at all temperatures. Beyond the portion shown, therefore, the wall would become completely vertical and it is not depicted because it would obscure the diagram. It is sufficient to show its behavior in the $T = 0$ plane. The crossings at $T = 0$ are not thermodynamic phase transitions, they merely indicate a change in the stable state as various sample parameters are changed.

Exploration of T_c and $\Delta\mathcal{F}(0)$ for larger values of D_F at several values of Λ indicates the existence of other 0- π boundaries at larger values of D_F . Thus, one could extend the phase diagram in that direction, but as previously seen⁶ and discussed above, these additional regions are qualitatively similar to the one shown here in detail, and quantitatively less interesting.

Computing a complete three dimensional phase diagram such as the one in Fig. 8 for a 7 layer system would be very expensive in computational resources and is not necessary. We have already seen in connection

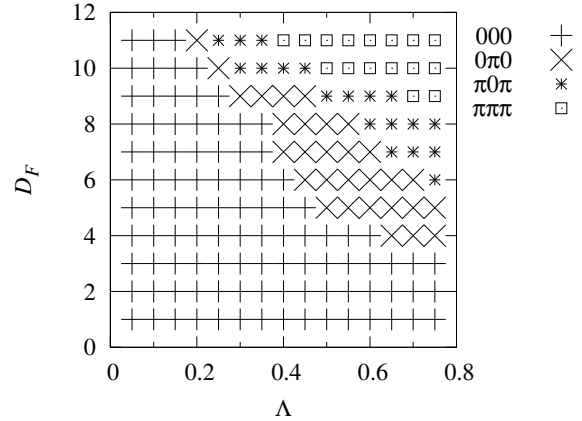


FIG. 9: The $T = 0$ plane of the phase diagram for the 7 layer system. The regions in which each of the four possible symmetric states is the stable one are indicated by the symbols in the legend. There are also metastable states at most values of Λ and D_F .

with Fig. 2 that first order transitions not only occur but are more abundant in such systems. Further evidence is in Fig. 9 where we show the zero temperature plane of the 7 layer phase diagram. A different symbol marks regions where each of the four possible symmetric states is the stable one at very low T . The many boundaries between the various states and the presence in many areas of metastable states (not marked) reflect that there may be many first order phase transitions in the 7 layer system. We can thus infer that even larger structures will

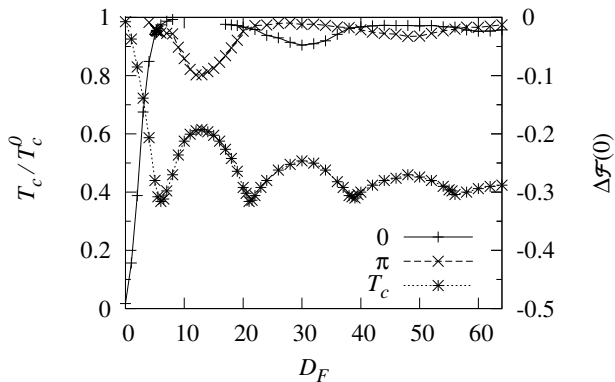


FIG. 10: T_c vs. D_F (left scale, * symbols) for $\Lambda = 0.70$. Also shown (right scale) are the energies of the 0 and π states at $T = 0$ (+ and \times signs respectively). Note the correlation between the changes in the stable state at $T = 0$ and the dips in T_c .

have rather intricate and rich phase diagram we found that the range of parameter space over which each type of transition persists is much broader than in the 3 layer case. For example, for a fixed $\Lambda = 0.55$, we observed phase transitions (see Fig. 2) between 000 and $0\pi0$ states for $4.4 < D_F < 5.0$, transitions between $0\pi0$ and $\pi0\pi$ for $7.75 < D_F < 8.0$ and transitions between $\pi0\pi$ and $\pi\pi\pi$ for $9.0 < D_F < 9.5$. For a fixed $D_F = 10$, the $\pi0\pi \leftrightarrow \pi\pi\pi$ transition exists³⁵ for $0.35 \leq \Lambda \leq 0.50$. We did not search for other transitions at $D_F = 10$.

By taking a slice of the phase diagram in Fig. 8 at fixed Λ , one can discern regular, damped oscillations of T_c with D_F . In Fig. 10 we show T_c for $\Lambda = 0.70$ over an extended range of D_F . It is clear that as D_F is increased the amplitude of the oscillations decreases. This is in good agreement with experiment, as we shall see in detail below. In addition to T_c , this figure shows $\Delta\mathcal{F}(0)$ for the 0 and π states. In a bulk superconductor, the ratio of this dimensionless quantity to the reduced transition temperature is -0.5 , which is confirmed here by our result for the 0 state at $D_F = 0$. The π state is unstable, for obvious reasons, in the $D_F \rightarrow 0$ limit. At finite values of D_F this relationship between normalized condensation energy and reduced transition temperature is not strictly obeyed, but there is a qualitative correlation: increases in the absolute value of $\Delta\mathcal{F}(0)$ correspond to increases in T_c . The values of D_F at which the stable state switches between 0 and π correspond to the sharp dips in T_c in all cases. This has also been seen in connection with Fig. 8 and it indicates that the structure and shape of the oscillations in T_c are strongly correlated with the low temperature state. The free energy data plotted have gaps, notably for the π state near $D_F \leq 4$ and for the 0 state at $8 \leq D_F \leq 17$. These values of D_F delimit regions in which the self-consistent calculation resulted in only one state. The free energy of the vanishing state goes continuously to zero at those boundaries. The pair amplitude is found to go also smoothly to zero.

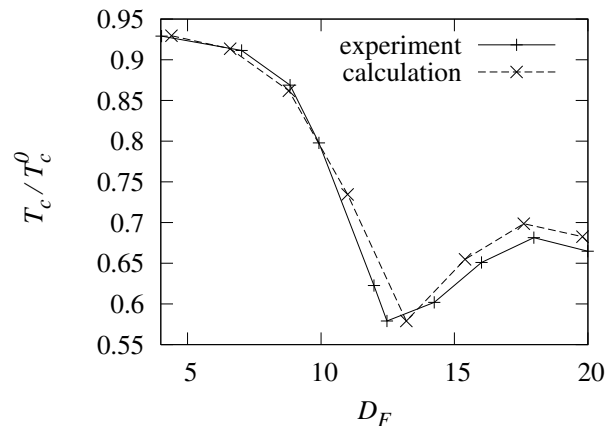


FIG. 11: Calculated values of T_c , in good agreement with experimental²⁰ data for a Nb/Co system. The experimental points shown are the average of the two series reported in Ref. 20.

The low temperature crossings at the many different values of D_F suggest the location of more $0 \leftrightarrow \pi$ phase transitions. This is in agreement with the direct observations reported in Ref. 24. Another corroboration of this claim comes from Ref. 16, in which the related parameter which they denote by I_c (the overall critical current of their nonuniform thickness junction) is found to have a significant dip at the $0 \leftrightarrow \pi$ transition temperature. Remarkably, these transitions were observed in Ref. 16 even though their samples did not have layers of uniform thickness. These two experiments and others show that this is an observable and robust phenomenon.

A similar analysis for the 7 layer case showed the same correspondence between $\Delta\mathcal{F}(0)$ and T_c . However, the larger number of energy crossings at $T = 0$ lead to a closer spacing of energy crossings in D_F , causing several local minima in $\Delta\mathcal{F}(0)$ to appear as a single broad minimum. The result was that multiple dips in T_c often merged. In larger systems, the existence of a broad local minimum in T_c may correspond to multiple crossings at low temperature.

F. Comparison with experiment

Many experimental groups^{20–24} have found oscillations in T_c as a function of F layer thickness. Our calculation also finds these oscillations (see Fig. 10). The agreement with experiment is furthermore quantitative. We show in Fig. 11 a direct comparison of our results to the experimental data for a Nb/Co system.²⁰ In the experiment, the spontaneous magnetization of the Co layer was found to depend on its thickness. This means, in our language, that I must be taken as a function of D_F for the purposes of this comparison. To do this, we fitted the spontaneous magnetization reported in Ref. 20 and extracted, at each thickness, the value of I from the formula below

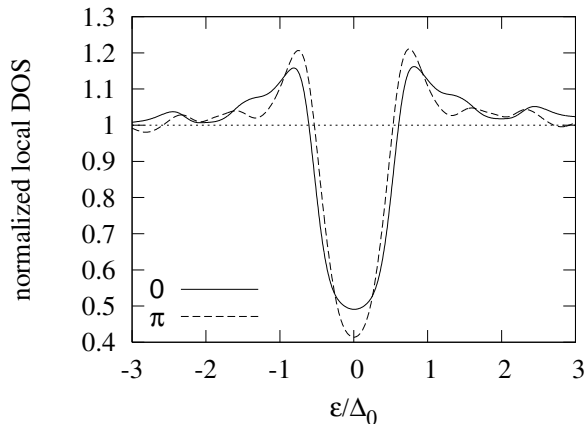


FIG. 12: Density of states at T_x for an SFS trilayer. The quantity plotted is the local DOS as defined in Eq. (2.6), averaged over an S layer, and normalized to the normal state bulk result in S. This is the case shown in the bottom left panel of Fig. 1 ($T_x/T_c^0 = 0.16$).

Eq. (2.8). We took a constant $\Lambda = 0.60$, which is appropriate to the materials mentioned. The experimental and theoretical values are in excellent quantitative agreement on the vertical scale, and the damped oscillations are well aligned in the thickness.

Comparing figures 11 and 10, we conclude that the dips in Fig. 11 must correspond to changes in the stable state at zero temperature. As these changes are, as we have seen, associated with the first order phase transitions, these dips in T_c may also be associated with first order phase transitions, in good agreement with what was reported in Ref. 24. This implies that studies of T_c may be a useful tool for experimental discovery of first order phase transitions and that samples which show dips in T_c are the ones that should be cooled down and studied to locate such phase transitions.

G. DOS and $M(z)$

Advanced tunneling spectroscopy techniques are a useful experimental tool to measure the local DOS, thus probing the single-particle spectrum. It has been found⁶ previously that the local DOS results for 0 and π states are different, including a modified subgap structure. In such cases, tunneling spectroscopy could be used to distinguish the states. We now investigate whether the density of states is also a suitable technique in locating phase transitions.

In Fig. 12 we show the DOS, defined as the normalized local DOS (from Eq. 2.6) averaged over one of the S layers, for a typical 3 layer system at the temperature where the first order transition occurs. The case shown is for the same parameters as in the bottom left panel of Fig. 1, with $T_x/T_c^0 = 0.16$. The energy is normalized to the bulk S gap at zero temperature, Δ_0 , while the DOS

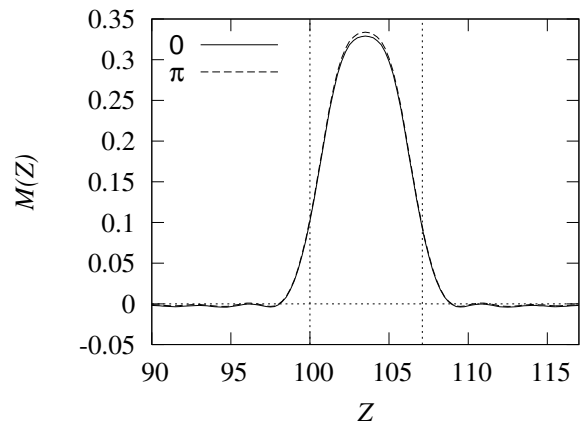


FIG. 13: The dimensionless local magnetization $M(Z)$ for an SFS trilayer at T_x . Only the central part of the sample is plotted. Results are given for the two nearly coexisting states. The case plotted is the same as in Fig. 12. The vertical dotted lines delimit the F region.

is normalized to its value in a bulk sample of S material in its normal state. For both 0 and π states maxima exist near the bulk gap edge, qualitatively reminiscent of the divergence found in a bulk superconductor. The local DOS never quite goes to zero in either state, demonstrating gapless superconductivity induced by the numerous Andreev bound states in the gap. The number of states in the gap is clearly larger for the 0 state and the peak is markedly lower. Although the DOS for both states have some general similarities, the differences that do exist are well within the resolution of current tunneling probes,³¹ making the DOS a potentially useful experimental technique in locating the phase transitions or identifying the stable state in the neighborhood of a transition.

The last quantity we shall briefly describe is the local dimensionless magnetization, $M(z)$, as defined in Eq. (2.8). Previous studies⁶ indicate that there is little difference between $M(z)$ for the 0 and π states at low temperature. In that case it was found that $M(z)$ was dominated by the exchange parameter I and was rather insensitive to the phase of the superconducting state. There was also little magnetization induced in the S region, as $M(z)$ decayed over the Fermi length scale.⁶ To illustrate the effect that temperature has on this trend, we show $M(Z)$ versus the dimensionless length Z at $T = T_x$ in Fig. 13. In the figure, the F region is delimited by vertical dotted lines and only a small portion of the S regions is shown. Consistent with Ref. 6, there is a quick decay and oscillation of $M(Z)$ in the S region. There is a rise in the value of $M(Z)$ to about 0.33 in the center of the F region, which is consistent with the bulk formula below Eq. (2.8) for $I = 0.2$. Indeed, as D_F increases $M(Z)$ flattens to a value that is in good agreement with that estimate. This is not contrary to the experimental results in Ref. 20 for which we modeled the change in the saturation magnetization with D_F by allowing for a D_F

dependent I , since in that case the magnetic properties (such the saturation magnetization) of the F layer were experimentally found to depend on D_F . Thus, the local magnetization, while interesting for other reasons, is not a good tool for determining the thermodynamically stable state or locating phase transitions.

IV. CONCLUSION

We have rigorously studied the thermodynamics of clean SFS trilayer junctions through self-consistent solutions to the BdG equations, in the clean limit. Building on previous work³⁵ where $0 \leftrightarrow \pi$ transitions in this system were found to be possible, we have computed here the three dimensional phase diagram of a clean SFS junction over an extended and physically relevant region of the space spanned by the parameters T , d_F , and Λ . We have found that the transition to the normal state is always of second order, while first order $\pi \rightarrow 0$ transitions occur, as temperature increases, over a range of Λ and D_F . Such transitions have been found experimentally. For systems consisting of three such junctions, we have found here that a variety of first order transitions, involving $0 \leftrightarrow \pi$ switching of one or more junctions, occur. The phase transitions were shown to be driven by a delicate balance between the condensation energy and the entropy. The absolute value of the pair amplitude is discontinu-

ous at the first order transition. Key elements of our approach are an efficient method to accurately compute free energies and a linearization scheme that calculates T_c . We have shown that dips in T_c overlap with regions in parameter space where phase transitions exist, which suggest that T_c studies should be useful for experimentally locating first order phase transitions. We have also calculated the variation of T_c with d_F and found good quantitative agreement with an experimental study²⁰ of a Nb/Co system. We have demonstrated that the phase transitions will have measurable latent heats, even for relatively small samples, over a broad range of magnet thicknesses. Another experimentally relevant quantity, the DOS, was calculated and deemed a potentially useful tool in locating phase transitions. The local magnetization, however, shows little difference between two states at the first order transition. The method and results demonstrated here are expected to be applicable to even larger structures.

V. ACKNOWLEDGMENTS

This work was supported in part by the University of Minnesota Graduate School and by the ARSC at the University of Alaska Fairbanks (part of the DoD HPCM program).

-
- * Electronic address: barsic@physics.umn.edu
 † Electronic address: otvalls@umn.edu
 ‡ Electronic address: klaus.halterman@navy.mil
 § Also at Minnesota Supercomputer Institute, University of Minnesota, Minneapolis, Minnesota 55455
 1 I. Žutić, J. Fabian, and S. Das Sarma, Rev. Mod. Phys. **76**, 323 (2004).
 2 A.F. Andreev, Sov. Phys. JETP **19**, 1228 (1964) [Z. Eksp. Teor. Fiz. **46**, 1823 (1964)].
 3 A.I. Buzdin, Rev. Mod. Phys. **77**, 935 (2005).
 4 E.A. Demler, G.B. Arnold, and M.R. Beasley, Phys. Rev. B **55**, 15174 (1997).
 5 V. N. Krivoruchko and E. A. Koshina, Phys. Rev. B **66**, 014521 (2002).
 6 K. Halterman and O.T. Valls, Phys. Rev. B **69**, 014517 (2004).
 7 K. Halterman and O.T. Valls, Phys. Rev. B **65**, 014509 (2002).
 8 A. Buzdin, Phys. Rev. B **62**, 11377 (2000).
 9 L.N. Bulaevskii, V. Kuzii, and A. Sobyenin, Pis'ma Zh. Eksp. Teor. Fiz. **25**, 314 (1977) [JETP Lett. **25**, 290 (1977)].
 10 V.V. Ryazanov, V.A. Oboznov, A.Y. Rusanov, A.V. Veretennikov, A.A. Golubov, and J. Aarts, Phys. Rev. Lett. **86**, 2427 (2001).
 11 H. Sellier, C. Baraduc, F. Lefloch, and R. Calemezuk, Phys. Rev. Lett. **92** 257005 (2004).
 12 S.M. Frolov, D.J. Van Harlingen, V.A. Oboznov, V. V. Bol'ginov, and V.V. Ryazanov, Phys. Rev. B **70**, 144505 (2004).

- 13 W. Guichard, M. Aprili, O. Bourgeois, T. Kontos, J. Lesueur, and P. Gandit, Phys. Rev. Lett. **90**, 167001 (2003).
 14 B. Jin, G. Su, and Q.R. Zheng, J. Appl. Phys., **96**, 5654 (2004).
 15 M.V. Milošević, G.R. Berdiyrov, and F.M. Peeters, Phys. Rev. Lett. **95**, 147004 (2005).
 16 S.M. Frolov, D.J. Van Harlingen, V. V. Bolginov, V.A. Oboznov, and V.V. Ryazanov, Phys. Rev. B **74**, 020503(R) (2006).
 17 T. Kontos, M. Aprili, J. Lesueur, F. Genêt, B. Stephanidis, and R. Boursier, Phys. Rev. Lett. **89**, 137007 (2002).
 18 V.A. Oboznov, V. V. Bol'ginov, A. K. Feofanov, V. V. Ryazanov, and A. I. Buzdin, Phys. Rev. Lett. **96**, 197003 (2006).
 19 V.L. Pokrovsky and H. Wei, Phys. Rev. B **69**, 104530 (2004).
 20 Y. Obi, M. Ikabe, T. Kubo, and H. Fujimori, Physica C **317-318**, 149 (1999).
 21 J.S. Jiang, D. Davidović, D.H. Reich, and C.L. Chien, Phys. Rev. Lett. **74** 314 (1995).
 22 J.S. Jiang, D. Davidović, D.H. Reich, and C.L. Chien, Phys. Rev. B **54**, 6119 (1996).
 23 Th. Mühge, N.N. Garif'yanov, Yu.V. Goryunov, G.G. Khaliullin, L.R. Tagirov, K. Westerholt, I.A. Garifullin, and H. Zabel, Phys. Rev. Lett. **77**, 1857 (1996).
 24 V. Shelukhin, A. Tsukernik, M. Karpovski, Y. Blum, K.B. Efetov, A.F. Volkov, T. Champel, M. Eschrig, T. Löfwander, G. Schön, and A. Palevski, Phys. Rev. B **73**,

- 174506 (2006).
- ²⁵ Z. Radović, N. Lazarides, and N. Flytzanis, Phys. Rev. B **68**, 014501 (2003).
- ²⁶ A. Radović, M. Lefvij, L. Dobrosavljević-Grujić, A. I. Buzdin, and J. R. Clem, Phys. Rev. B **44**, 759 (1991).
- ²⁷ B. Krunavakarn and S. Yoksan, Physica C **440**, 25 (2006).
- ²⁸ A.I. Buzdin, L.N. Bulaevskii, and S.V. Panyukov, Pis'ma Zh. Eksp. Teor. Fiz. **35**, 147-148 (1982). [JETP Lett **35**, 178-180 (1982)].
- ²⁹ A.I. Buzdin and M.Yu. Kuprianov, Pis'ma Zh. Eksp. Teor. Fiz. **53**, 308-312 (1991) [JETP Lett. **53**, 321-326 (1991)].
- ³⁰ A. Buzdin and I. Baladié, Phys. Rev. B **67**, 184519 (2003).
- ³¹ T. Kontos, M. Aprili, J. Lesuer, and X. Grison, Phys. Rev. Lett. **86**, 304 (2001).
- ³² S. Raymond, P. SanGiorgio, M.R. Beasley, J. Kim, T. Kim, and K. Char, Phys. Rev. B **73**, 054505 (2006).
- ³³ L. Crétninon, A.K. Gupta, H. Sellier, F. Lefloch, M. Fauré, A. Buzdin, and H.Courtois, Phys. Rev. B **72**, 024511 (2005).
- ³⁴ K. Halterman and O.T. Valls, Phys. Rev. B **70**, 104516 (2004).
- ³⁵ P.H. Barsic, O.T. Valls and K. Halterman, Phys. Rev. B **73**, 144514 (2006).
- ³⁶ S. Tollis, Phys. Rev. B **69**, 104532 (2004).
- ³⁷ K. Halterman and O.T. Valls, Phys. Rev. B **66**, 224516 (2002).
- ³⁸ J. Cayssol and G. Montambaux, Phys. Rev. B **71**, 012507 (2005).
- ³⁹ A. Buzdin, Phys. Rev. B **72**, 100501(R) (2005).
- ⁴⁰ P.G. de Gennes, *Superconductivity of Metals and Alloys* (Addison-Wesley, Reading, MA, 1989).
- ⁴¹ I. Kosztin, Š. Kos, M. Stone, and A.J. Leggett, Phys. Rev. B **58**, 9365 (1998).
- ⁴² M. Tinkham, *Introduction to Superconductivity, 2d. ed.* (Dover Publications, June 2004).
- ⁴³ P.B. Allen and R.C. Dynes, Phys. Rev. B **12**, 905 (1975).
- ⁴⁴ K. Levin and O.T. Valls, Phys. Rev. B **17**, 191 (1978).
- ⁴⁵ B.P. Stojković and O.T. Valls Phys. Rev. B **49**, 3413 (1994); Phys. Rev. B **50**, 3374 (1994), and references therein.
- ⁴⁶ See for example, page 451 of A.L. Fetter and J.D. Walecka, *Quantum Theory of Many-Particle systems*, McGraw-Hill, New York (1971).
- ⁴⁷ C.C. Huang, private communication.
- ⁴⁸ O. Bourgeois, S.E. Skipetrov, F.Ong, and J. Chaussy, Phys. Rev. Lett. **94**, 057007 (2005).